Supporting Information

Theoretical analysis of characteristic in $BeMgCu_4$ cluster and its implication for CO_2 activation

Lifang Yan [a], Xingman Liu [a,], Yue Huang [a], Xinluo Wu [a] , Xiaomeng Wang[a,]* and Zhongmin Su [b, c,]**

Address:

[a] School of Chemistry and Chemical Engineering, School of Physics, Ningxia University, Yinchuan 750021, China

[b] State Key Laboratory of Supramolecular Structure and Materials, Institute of Theoretical Chemistry, College of Chemistry, Jilin University, Changchun 130021, China

[c] Institute of Functional Material Chemistry, Faculty of Chemistry & National & Local United Engineering Laboratory for Power Battery, Northeast Normal University, Changchun 130024, China

*Corresponding Authors:

E-mail address:

liuxm2020@nxu.edu.cn (X. M. Liu); xiaomengwang@nxu.edu.cn; zmsu@nenu.edu.cn (Z. M. Su);

Table of Contents

SI1

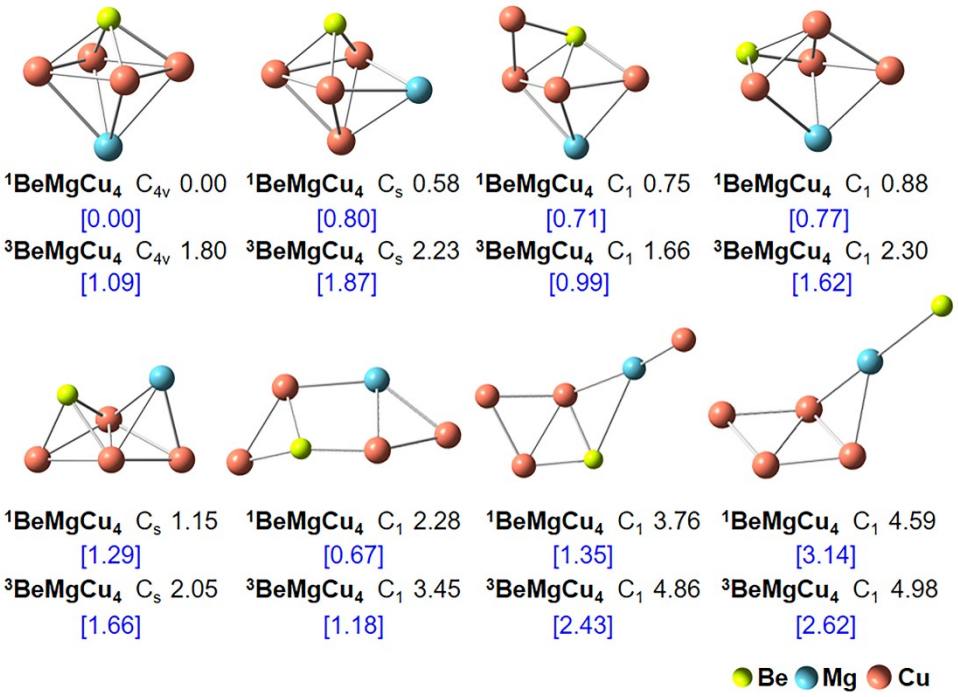

Fig. S1 The relative energies of the different isomers of the $BeMgCu_4$ clusters. The structures were searched by the ABCluster program, followed by rigorous geometry optimization using Gaussian 09 at the B3LYP/6-31G(d) level. The point group is given under each structure, and the superscripts indicate the spin multiplicities. The energy values (eV) shown in blue were calculated at the CCSD/6-311G(d) level, demonstrating strong agreement with DFT results. These calculations identified the singlet-state C_{4v}-$BeMgCu_4$ as the global minimum structure.

SI2

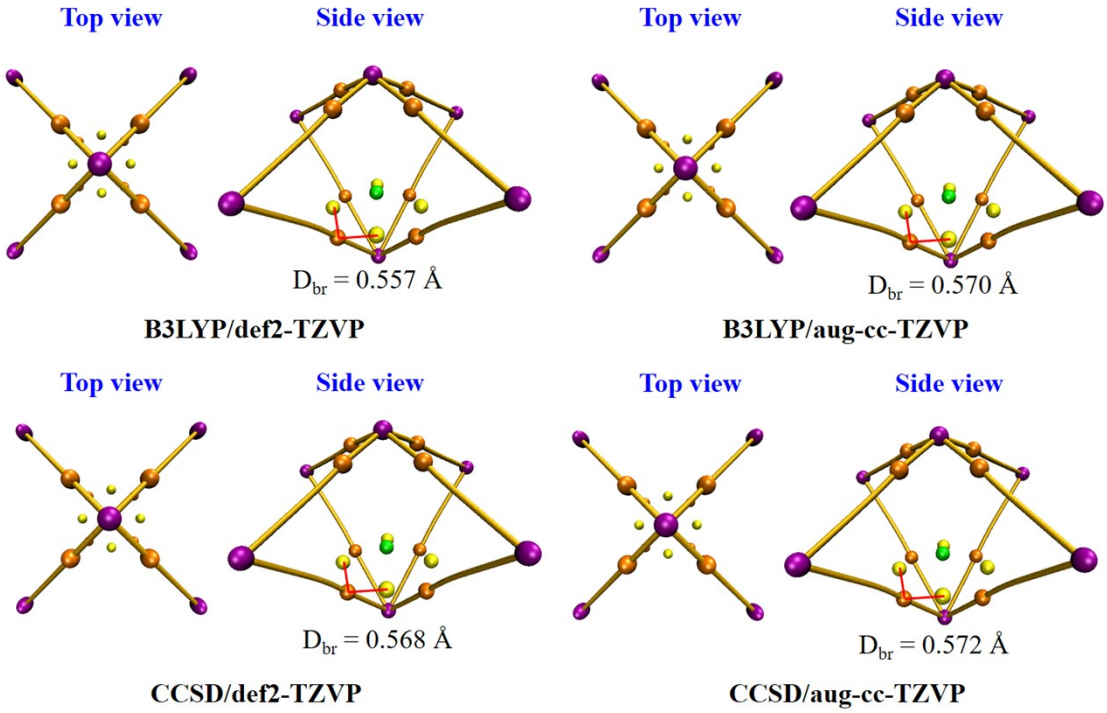

Fig. S2 The AIM topological analysis mapping of C_{4v}-$BeMgCu_4$. The purple, orange, yellow, and green points represent the positions of the nuclear critical point (NCP), the bond critical point (BCP), the ring critical point (RCP), and the cage critical point (CCP), respectively. D_{br} indicates the distance between the BCP and its nearest RCPs.

	Cu4	Be	Mg	Sum (BeMg)
HOMO	25.8%	26.2%	48.0%	74.2%
HOMO-1	53.5%	37.8%	8.7%	46.5%
HOMO-2	58.4%	26.7%	14.9%	41.6%
HOMO-17	83.5%	14.3%	2.2%	16.5%

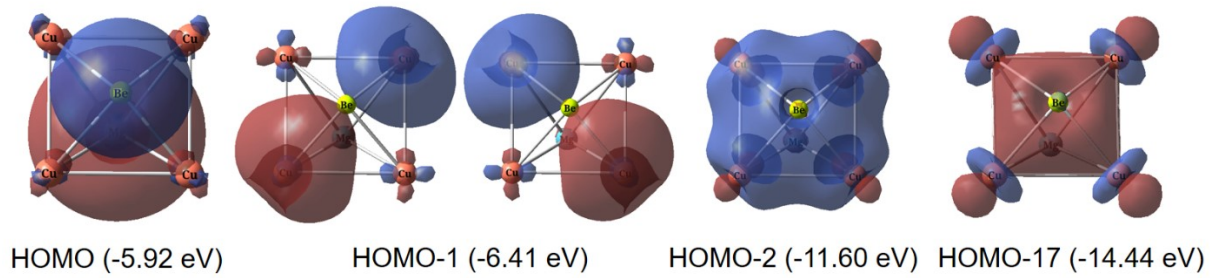

Fig. S3 Important front molecular orbital and composition of C_{4v}-$BeMgCu_4$ at the CCSD/6-311G(d)/LANL2DZ level (isovalue = 0.04). 6-311G(d) for Be and Mg, while LANL2DZ for Cu.

SI3

	Cu4	Be	Mg	Sum (BeMg)
HOMO	31.2%	25.7%	43.1%	68.8%
HOMO-1	65.7%	28.6%	5.7%	34.3%
HOMO-17	54.5%	34.8%	10.7%	45.5%

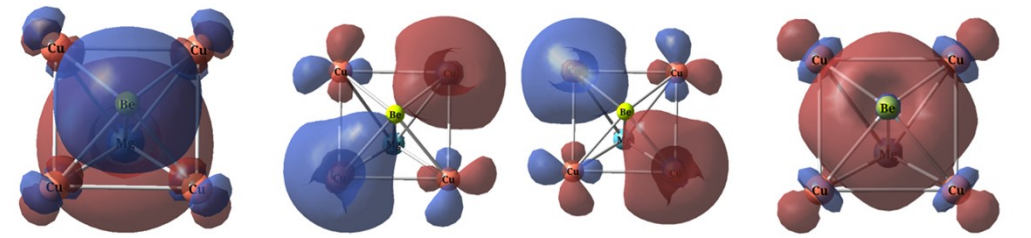

HOMO (-5.07 eV) HOMO-1 (-5.53 eV) HOMO-17 (-10.49 eV)

Fig. S4 Important front molecular orbital and composition of C_{4v}-$BeMgCu_4$ at the B3LYP/6-311++G(d, p) level (isovalue = 0.04).

	Cu4	Be	Mg	Sum (BeMg)
HOMO	17.9%	32.0%	50.1%	82.1%
HOMO-1	65.8%	25.8%	8.4%	34.2%
HOMO-17	50.7%	37.5%	11.8%	49.3%

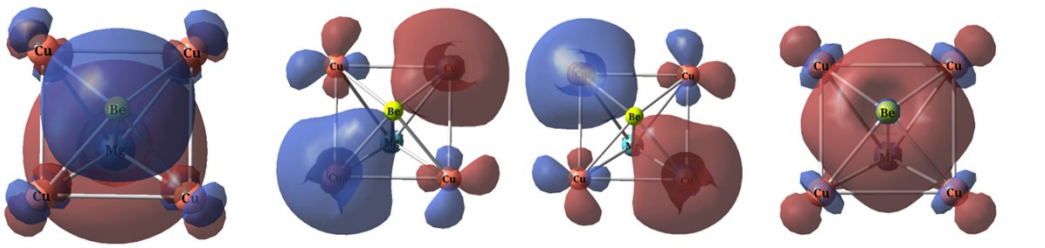

HOMO (-5.08 eV) HOMO-1 (-5.52 eV) HOMO-17 (-10.49 eV)

Fig. S5 Important front molecular orbitals and composition of C_{4v}-$BeMgCu_4$ at the B3LYP/def2-TZVP level (isovalue = 0.04).

SI4

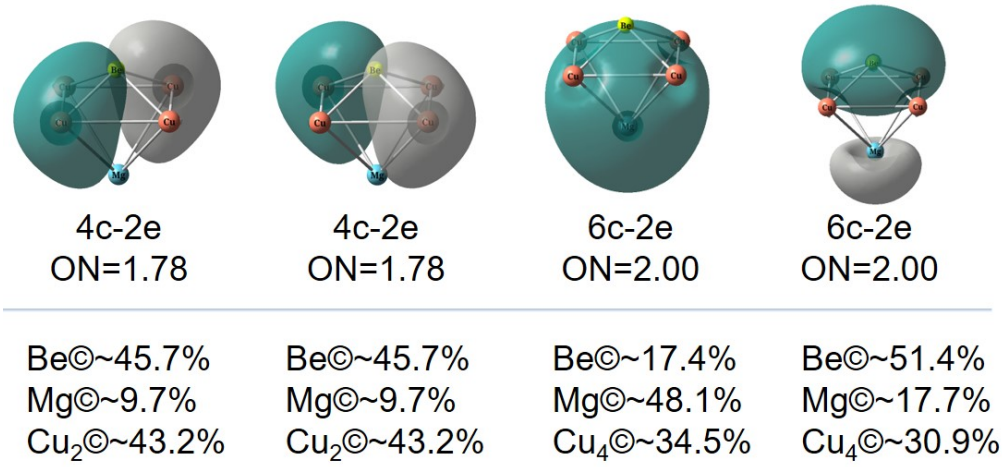

Fig. S6 Schematic representation of the AdNDP patterns for C_{4v}-$BeMgCu_4$ at the CCSD/6-311G(d)/LANL2DZ level (isovalue = 0.04).

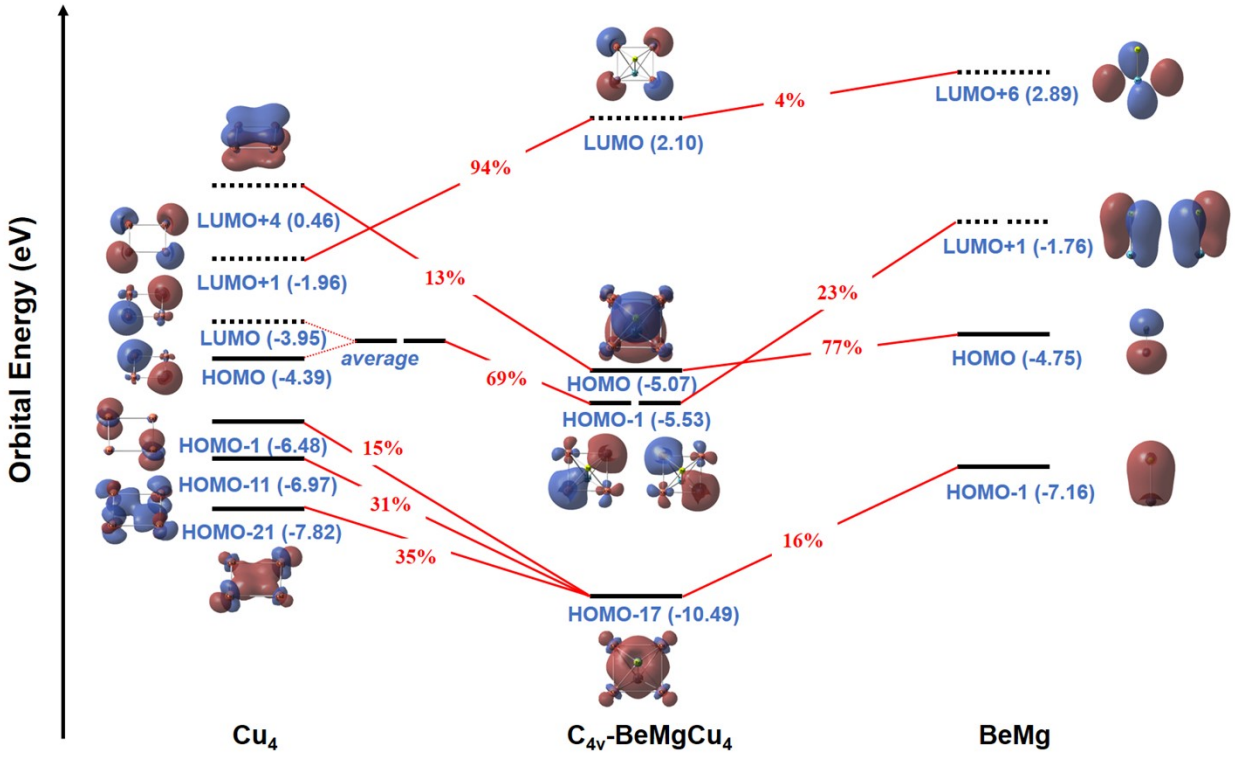

Fig. S7 The dominant FMO correlation diagram of C_{4v}-$BeMgCu_4$ between BeMg and Cu_4 fragments calculated at the B3LYP/def2-TZVP level. The horizontal dashed and solid lines represent virtual and occupied molecular orbitals, respectively (the orbital energies are also given in brackets, unit: eV). It can be observed that the π orbitals of Be-Mg (LUMO+1) contribute 23% to the Be-Mg delocalized double π interaction (HOMO-1) in C_{4v}-$BeMgCu_4$.

SI5

(a) ^{3}[BeMg]^{0} + ^{3}[Cu4] ^{0}

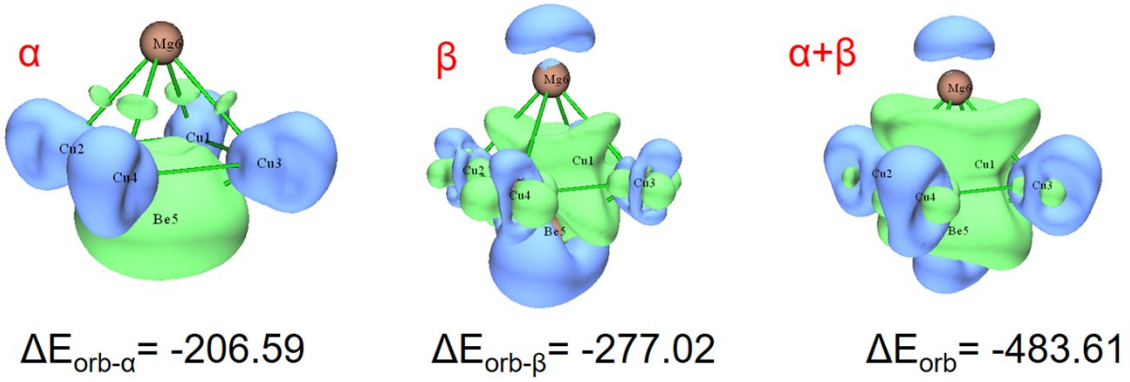

(b) ^{5}[BeMg]^{0} + ^{5}[Cu4] ^{0}

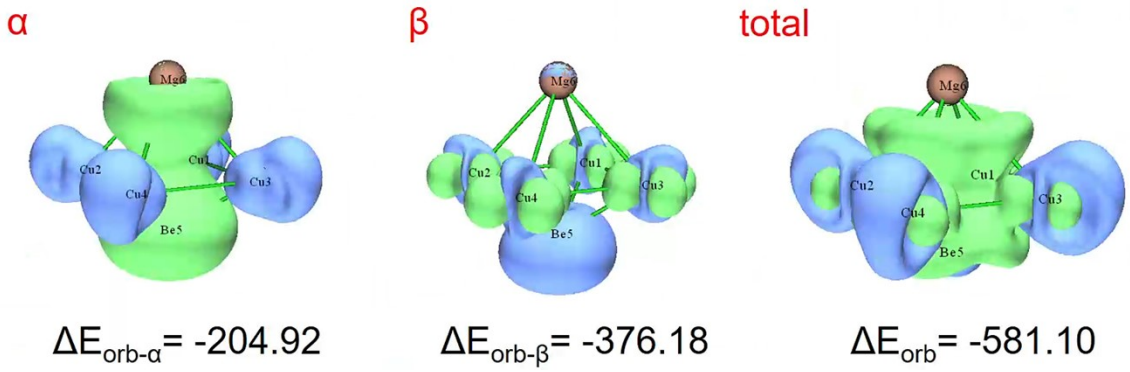

Fig. S8 Schematic representation of the important bonding NOCV pair orbitals in $BeMgCu_4$ based on two fragments Cu_4 and BeMg at the B3LYP/6-311G(d) level (charge flow is blue → green. Isosurface value = 0.005 a.u.. Energy values are given in kcal/mol.)

SI6

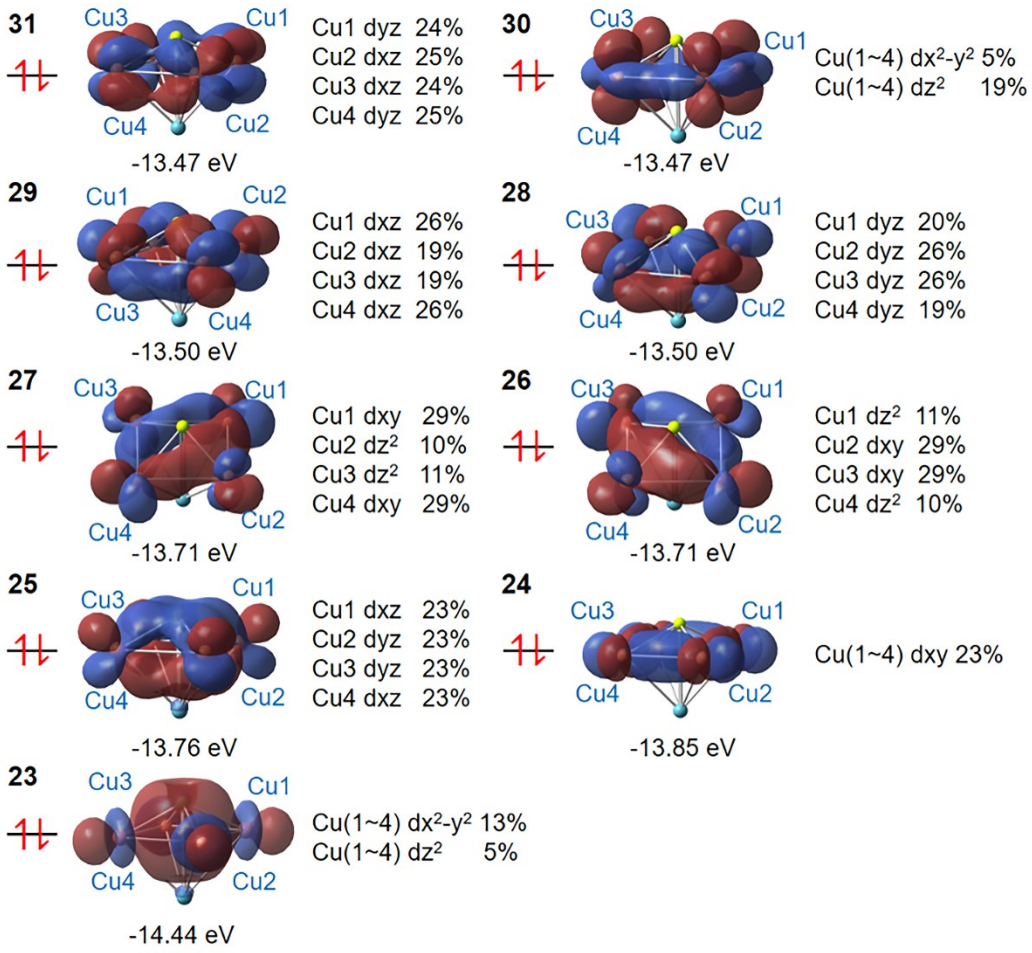

Fig. S9 The occupied molecular orbitals diagram bonded mainly by the d orbitals of four copper atoms at the CCSD/6-311G(d)/LANL2DZ level (isovalue = 0.02). The contribution of d orbitals from each copper atom to the corresponding bonding molecular orbitals was determined by aggregating the basis functions.

SI7

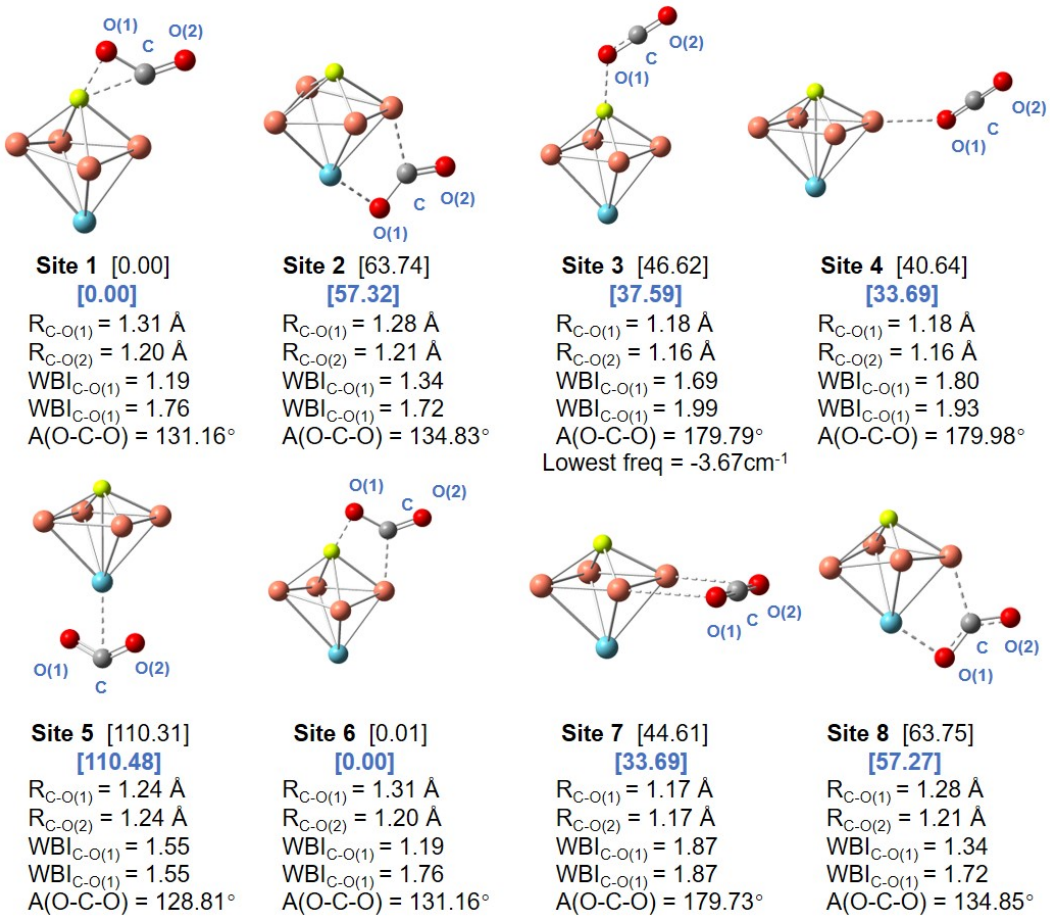

Fig. S10 The carbon end of CO_2 attacks the eight sites of the $BeMgCu_4$ cluster in a parallel manner. The bond length, bond angle, and bond level data of CO_2 was calculated at the B3LYP/6-31G(d)/LANL2DZ level using the DFT method. The zero-point vibration corrected energies (kJ/mol) of each structure are given in the square brackets. The energies (kJ/mol) in blue were calculated at B3LYP/def2-TZVP level, which isconsistent with the results of another method calculation at B3LYP/6-31G(d)/LANL2DZ level.

SI8

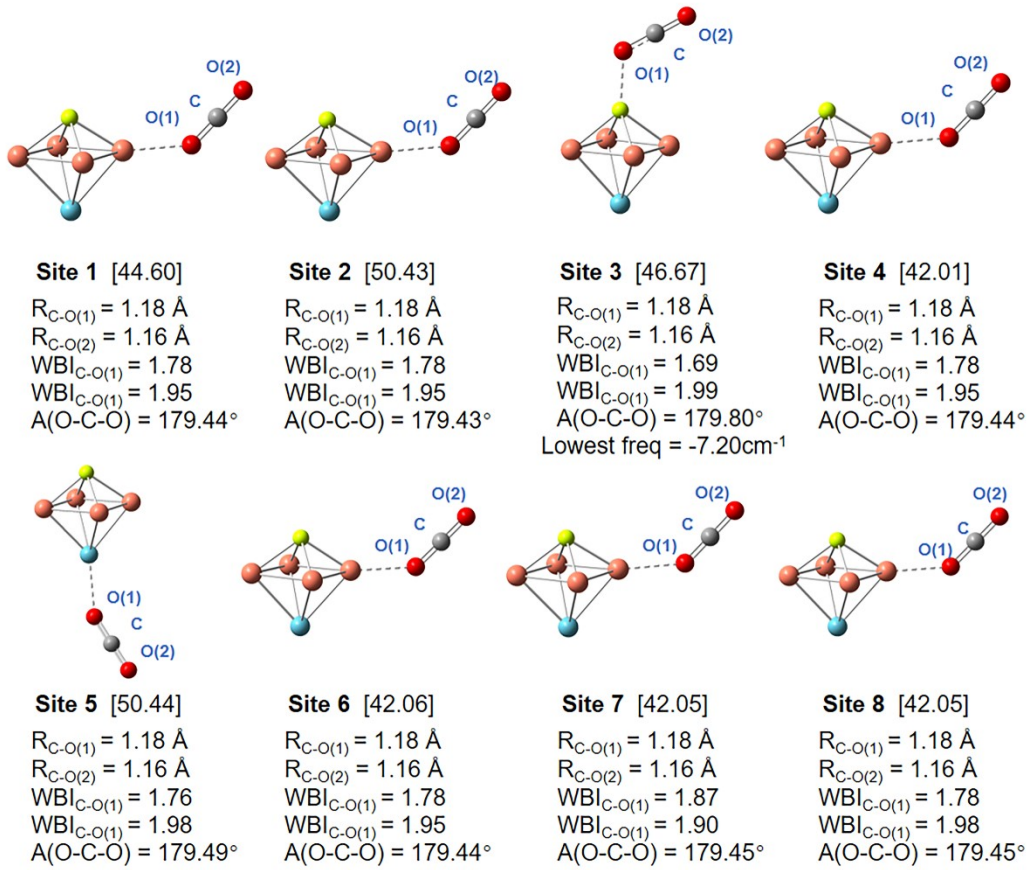

Fig. S11 The oxygen end of CO_2 attacks the eight sites of the $BeMgCu_4$ cluster in a vertical manner. The bond length, bond angle, and bond level data of CO_2 was calculated at the B3LYP/6-31G(d)/LANL2DZ level using the DFT method. The zero-point vibration corrected energies (kJ/mol) of each structure are given in the square brackets.

SI9

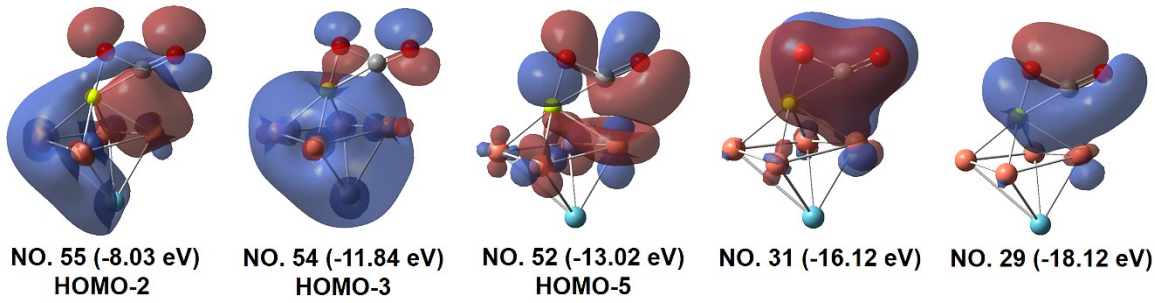

Fig. S12 The main frontier molecular orbitals of $BeMgCu_4$-CO_2 at the CCSD/6-311G(d)/LANL2DZ level. Isosurface value = 0.02 a.u..

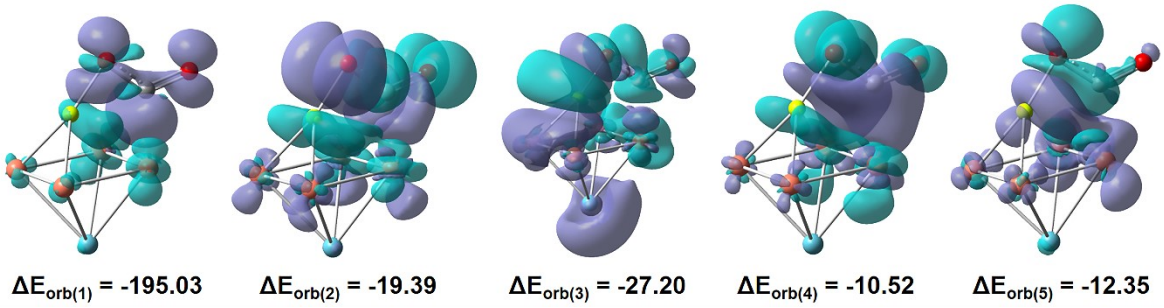

Fig. S13 Schematic representation of the important bonding NOCV pair orbitals in $BeMgCu_4$-CO_2 based on two fragments $BeMgCu_4$ and CO_2 at the B3LYP/6-31G(d) level (charge flow is blue → pink. Isosurface value = 0.005 a.u. (1), 0.0005 a.u. (2-5). Energy values are given in kcal/mol.)

SI10

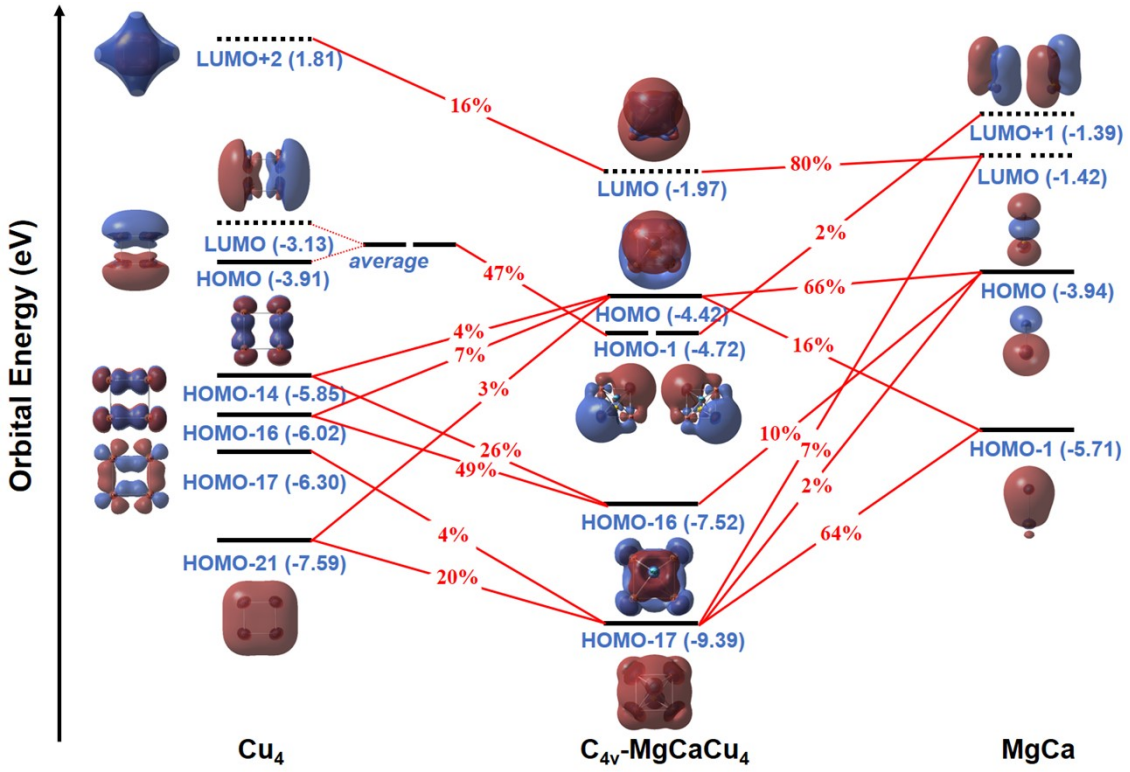

Fig. S14 The dominant FMO correlation diagram of C_{4v}-$MgCaCu_4$ between MgCa and Cu_4 fragments calculated at the B3LYP/6-311G(d) level. The horizontal dashed and solid lines represent virtual and occupied molecular orbitals, respectively (the orbital energies are also given in brackets, unit: eV).

SI11

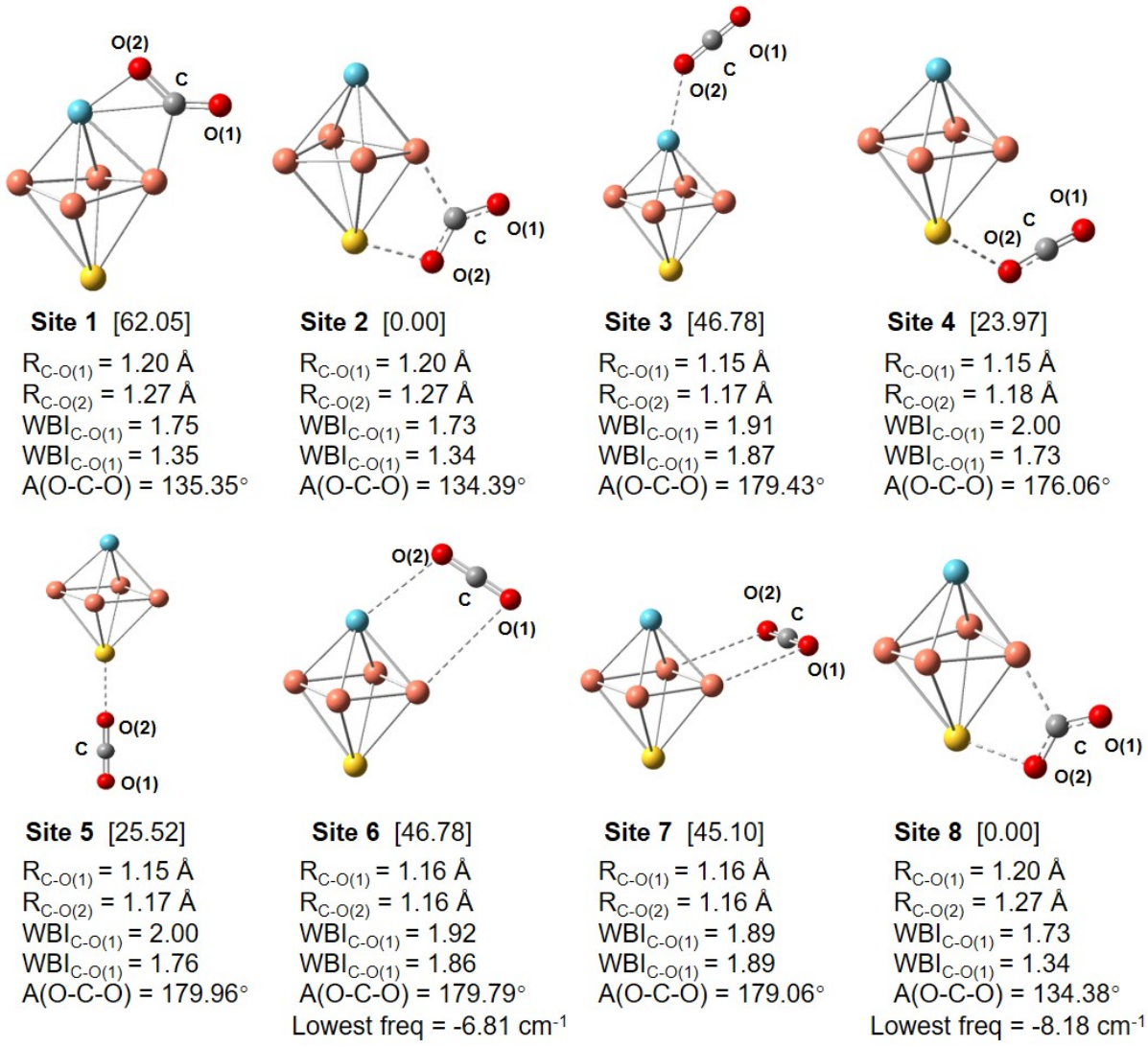

Fig. S15 The carbon end of CO_2 attacks the eight sites of the $MgCaCu_4$ cluster in a parallel manner. The bond length, bond angle, and bond level data of CO_2 was calculated at the B3LYP/6-31G(d)/LANL2DZ level using the DFT method. The zero-point vibration corrected energies (kJ/mol) of each structure are given in the square brackets.

SI12

Table S1 The crucial occupied molecular orbitals composition of **C_{4v}-BeMgCu_4**. The coefficient of each orbital is given by the contribution from the fragments. Calculations at CCSD/6-311G(d)/LANL2DZ level.

Diagram	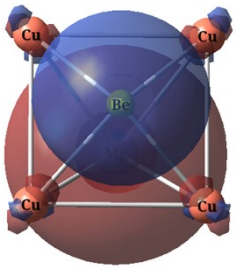	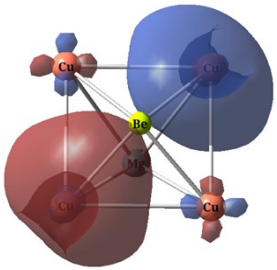	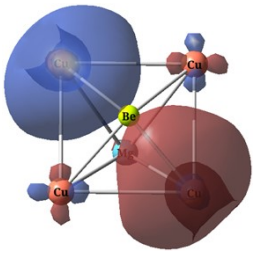	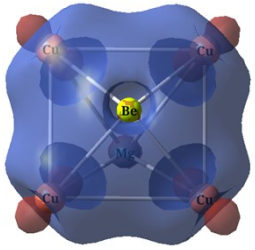	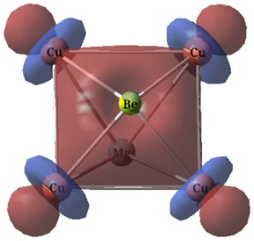
Energy/eV	-5.92	-6.41		-11.60	-14.44
Component	Cu4©~4p 22.5% Cu4©~3d 3.1% Be©~2s 19.6% Be©~2p 6.2% Mg©~3s 44.2% Mg©~3p 2.5%	Cu4©~4p 11.2% Cu4©~3d 2.1% Cu4©~4s 37.5% Be©~2p 37.7% Mg©~3p 8.5%	Cu4©~4p 11.2% Cu4©~3d 2.1% Cu4©~4s 37.5% Be©~2p 37.7% Mg©~3p 8.5%	Cu4©~4s 25.2% Cu4©~4p 9.2% Cu4©~3d 21.7% Be©~2s 22.6% Be©~2p 3.3% Mg©~3s 11.7% Mg©~3p 2.3%	Cu4©~4s 25.2% Cu4©~4p 9.2% Cu4©~3d 21.7% Be©~2s 22.6% Be©~2p 3.3% Mg©~3s 11.7% Mg©~3p 2.3%

SI13

Table S2 The crucial occupied molecular orbitals composition of **C_{4v}-BeMgCu_4**. The coefficient of each orbital is given by the contribution from the fragments. Calculations at B3LYP/6-311++G(d, p) level.

Diagram	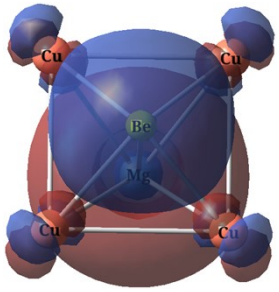	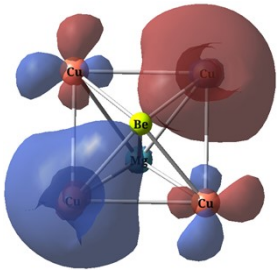	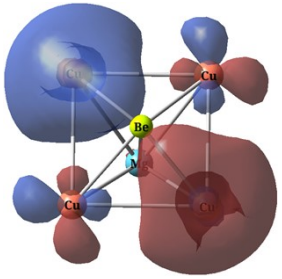	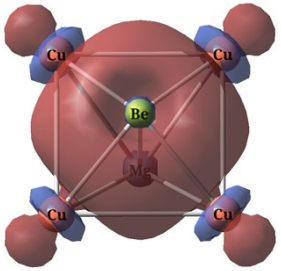
Energy/eV	-5.07	-5.53		-10.49
Component	Cu_4©~4p 21.4% Cu_4©~3d 9.2% Be©~2s 18.2% Be©~2p 7.2% Mg©~3s 39.5% Mg©~3p 2.4%	Cu_4©~4s 40.0% Cu_4©~4p 7.5% Cu_4©~3d 15.4% Be©~2p 28.6% Mg©~3p 5.6%	Cu_4©~4s 40.0% Cu_4©~4p 7.5% Cu_4©~3d 15.4% Be©~2p 28.6% Mg©~3p 5.6%	Cu_4©~4s 21.2% Cu_4©~4p 8.6% Cu_4©~3d 21.9% Be©~2s 25.6% Be©~2p 8.1% Mg©~3s 6.9% Mg©~3p 3.0%

SI14

Table S3 The crucial occupied molecular orbitals composition of **C_{4v}-$BeMgCu_4$**. The coefficient of each orbital is given by the contribution from the fragments. Calculations at B3LYP/def2-TZVP(d, p) level.

Diagram	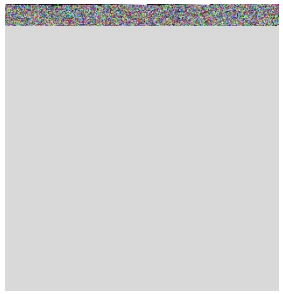			
Energy/eV	-5.07	-5.53		-10.49
Component	Cu_4©~4p 7.2% Cu_4©~3d 9.3% Be©~2s 21.0% Be©~2p 10.7% Mg©~3s 46.3% Mg©~3p 4.1%	Cu_4©~4s 45.0% Cu_4©~4p 3.8% Cu_4©~3d 15.6% Be©~2p 25.8% Mg©~3p 8.4%	Cu_4©~4s 45.0% Cu_4©~4p 3.8% Cu_4©~3d 15.6% Be©~2p 25.8% Mg©~3p 8.4%	Cu_4©~4s 23.0% Cu_4©~4p 3.4% Cu_4©~3d 21.8% Be©~2s 29.1% Be©~2p 7.5% Mg©~3s 7.9% Mg©~3p 3.3%

SI15

Table S4 Atomic charges of some small molecules calculated by different methods at B3LYP/6-311G(d).

Molecular	Atom	Mulliken	Hirshfeld	ADCH	NPA	MK	AIM
C_{4v}-$BeMgCu_4$	Be	-1.222	-0.208	-0.385	-1.259	-0.338	1.209
	Mg	-0.907	-0.010	-0.094	-0.338	-0.089	0.730
	Cu	0.532	0.055	0.120	0.099	0.107	-0.485
C_{4v}-$BeMgLi_4$	Be	-0.101	-0.370	-0.764	-1.933	-0.766	-2.996
	Mg	-0.165	-0.098	-0.334	-0.092	-0.341	-0.134
	Li	0.067	0.117	0.275	0.507	0.277	0.783
C_{4v}-$MgCaCu_4$	Mg	-0.943	0.014	0.112	-0.507	0.151	0.834
	Ca	-0.376	0.147	0.316	0.105	0.503	0.796
	Cu	0.330	-0.040	-0.082	0.100	-0.164	-0.407
C_{4v}-$MgCaLi_4$	Mg	-0.171	-0.145	-0.280	-0.995	-0.209	-2.598
	Ca	0.190	-0.029	-0.096	0.252	0.097	-0.186
	Li	-0.005	0.044	0.094	0.186	0.028	0.696
D_{4h}-Be_2Cu_4	Be	-1.277	-0.224	-0.500	-1.084	-0.488	1.084
	Cu	0.639	0.112	0.250	0.542	0.245	-0.542
D_{4h}-Be_2Li_4	Be	-0.186	-0.321	-0.691	-1.201	-0.708	-1.282
	Li	0.093	0.160	0.346	0.600	0.354	0.810
D_{4h}-Mg_2Cu_4	Mg	-0.186	0.042	0.052	-0.393	0.091	0.881
	Cu	0.408	-0.021	0.026	0.197	-0.046	-0.440
D_{4h}-Mg_2Li_4	Mg	-0.114	-0.127	-0.292	-0.587	-0.342	-0.481
	Li	0.057	0.063	0.146	0.294	0.171	0.740
D_{4h}-Ca_2Cu_4	Ca	-0.476	0.112	0.252	0.021	0.518	0.724
	Cu	0.238	-0.056	-0.126	-0.010	0.259	-0.362
C_{2v}-Ca_2Li_4	Ca	0.268	-0.031	-0.005	0.111	0.097	-0.103
	Li	-0.134	0.015	0.003	-0.055	-0.048	0.292

SI16

Table S5 The $BeMgCu_4$-CO_2 structures. CO_2 was selected as the probe molecule to attack the eight different sites of octahedral cluster in both vertical (O-terminus) and parallel (C-terminus). The sixteen initial structures were optimized at the B3LYP/6-31G(d)/LANL2DZ level using DFT method.

Site	Parallel (C-terminus)		Vertical (O-terminus)	
	Initial structure	Optimized structure	Initial structure	Optimized structure
1	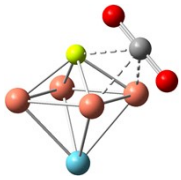	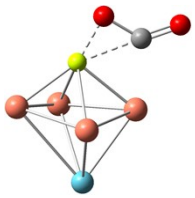	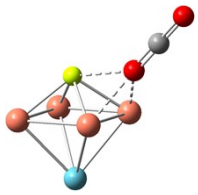	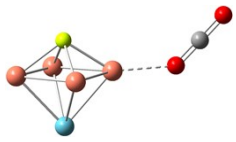
2	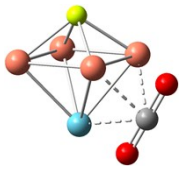	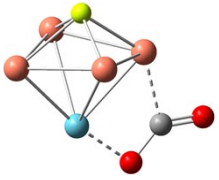	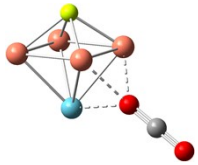	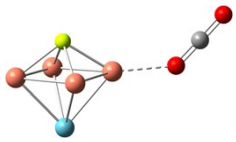
3	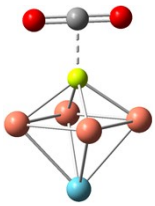	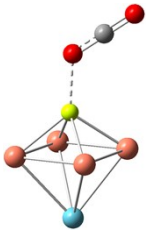	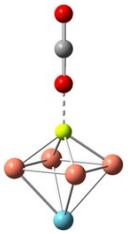	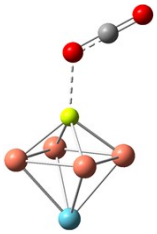
4	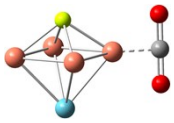	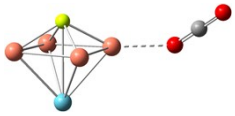	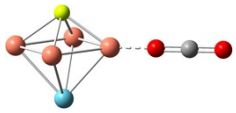	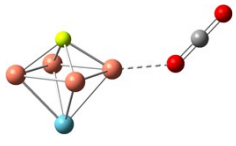

Site	Parallel (C-terminus)		Vertical (O-terminus)	
	Initial structure	Optimized structure	Initial structure	Optimized structure
5	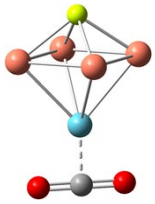	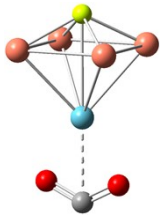	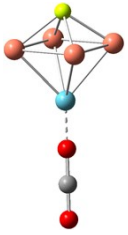	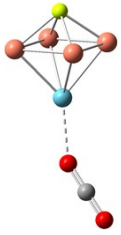
6	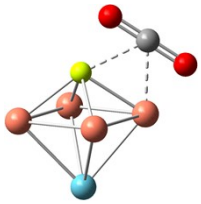	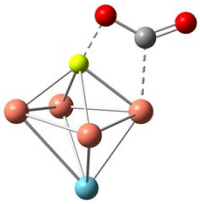	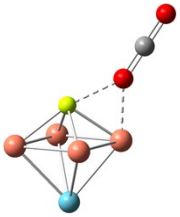	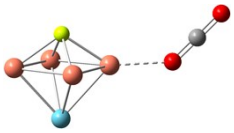
7	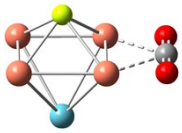	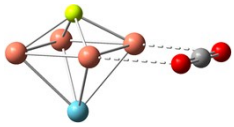	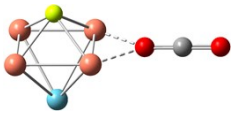	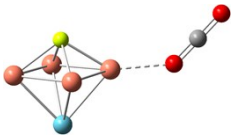
8	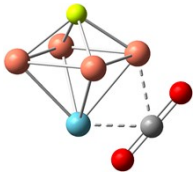	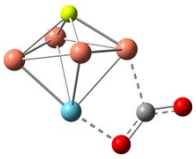	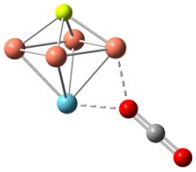	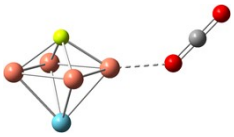

SI17

Table S6 The properties of CO_2 were calculated at CCSD/6-311G(d)/LANL2DZ level of theory.

Property	Bond Angle	R_{C-O} (Å)	WBI_{C-O}	NPA (|e|)	SVF_{C-O} (cm^{-1})	FC_{C-O}
[a] CO_2	180.00°	1.16	1.75	C: 1.01 O: -0.51	2454.81	16.67
[b] CO_2	131.39°	C-O(1): 1.31 C-O(2): 1.20	C-O(1): 1.09 C-O(2): 1.60	C: 0.58 O(1): -0.76 O(2): -0.53	1810.59	C-O(1): 5.43 C-O(2): 12.05

Superscripts are employed to differentiate CO_2 molecules pre- and post-activation. Notations: a – unactivated CO_2, b – activated CO_2 at site 1.

Table S7 Cartesian coordinates of C_{4v}-$BeMgCu_4$ obtained at the CCSD/6-311G(d)/LANL2DZ level.

Coordinate (Å) **^{1}BeMgCu$_4$**			
Cu	1.95380100	0.00000000	-0.14463000
Cu	0.00000000	1.95380100	-0.14463000
Cu	0.00000000	-1.95380100	-0.14463000
Cu	-1.95380100	0.00000000	-0.14463000
Be	0.00000000	0.00000000	-1.08286900
Mg	0.00000000	0.00000000	1.76207000